

# New Developments in Multi-Filter Rotating Shadowband Radiometer Data Analysis

*M. Alexandrov and B. Cairns  
Columbia University  
New York, New York*

*A.A. Lacis and B.E. Carlson  
National Aeronautics and Space Administration-Goddard Institute for Space Studies  
New York, New York*

## Introduction

We present further development of our analysis algorithm (Alexandrov et al. 2005) for multi-filter rotating shadowband radiometer (MFRSR) data. The new additions include a study of MFRSR retrievals sensitivity to ill-constrained nitrogen dioxide column amount, and techniques allowing us to retrieve spectral aerosol single-scattering albedo (SSA) and column amount of precipitable water vapor (PWV). The SSA retrievals employ MFRSR measurements of both direct normal and diffuse horizontal irradiances. The algorithm has been tested on a long-term dataset from the local MFRSR network at the Department of Energy's ARM Climate Research Facility (ACRF) Southern Great Plains (SGP) site. Our results are compared to Aerosol Robotic Network's (AERONET) almucantar scan retrievals of SSA from CIMEL sun-photometer co-located with the MFRSR at the SGP Central Facility. Precipitable water vapor column amounts are determined from the direct normal irradiances in the 940 nm MFRSR spectral channel. HITRAN 2004 spectral database has been used to model the water vapor absorption, while a range of other databases (HITRAN 1996, 2000, European Space Agency [ESA]) has been used in sensitivity study. The results of the PWV retrievals for SGP's MFRSR network are compared with correlative measurements by microwave radiometers (MWR), Global Positional System (GPS) station, and AERONET. Spatial structure of PWV field reconstructed by interpolation of MFRSR-derived values from the whole SGP network has been compared with that of moderate-resolution imaging spectroradiometer (MODIS) PWV satellite product.

## Sensitivity of MFRSR-Derived Aerosol Parameters to the Assumed NO<sub>2</sub> Column Amount

Given the spectral range (400 - 600 nm) of NO<sub>2</sub> absorption in the visible part of the spectrum, this absorption, if neglected by a retrieval algorithm is, in fact, misinterpreted as a contribution from very

small aerosol particles. This effectively decreases the retrieved size of fine mode aerosol. However, this is not the sole effect of underestimating  $\text{NO}_2$  on retrieved aerosol parameters. Indeed, the underestimating the retrieved fine mode size affects the whole aerosol extinction spectrum including the longwave spectral region outside  $\text{NO}_2$  absorption band. The increase of aerosol optical thicknesses (AOTs) spectral slope in this region associated with a decrease in size is compensated by an increase in the coarse mode fraction in AOT so that the longwave Angstrom exponent remains intact. To illustrate this effect, Figure 1 shows the scatter plots of the values of fine mode fraction in 870 nm AOT obtained using both constrained (zero  $\text{NO}_2$ ) and unconstrained retrieval methods. These plots show that constraining  $\text{NO}_2$  to zero for E2, which has significant  $\text{NO}_2$  amounts in unconstrained retrievals, leads to significant decrease in fine mode fraction, thus the coarse particles now effectively replace large-size fine mode in keeping the longwave Angstrom exponents low. For other sites (e.g. E13) the differences in fine fraction are smaller.

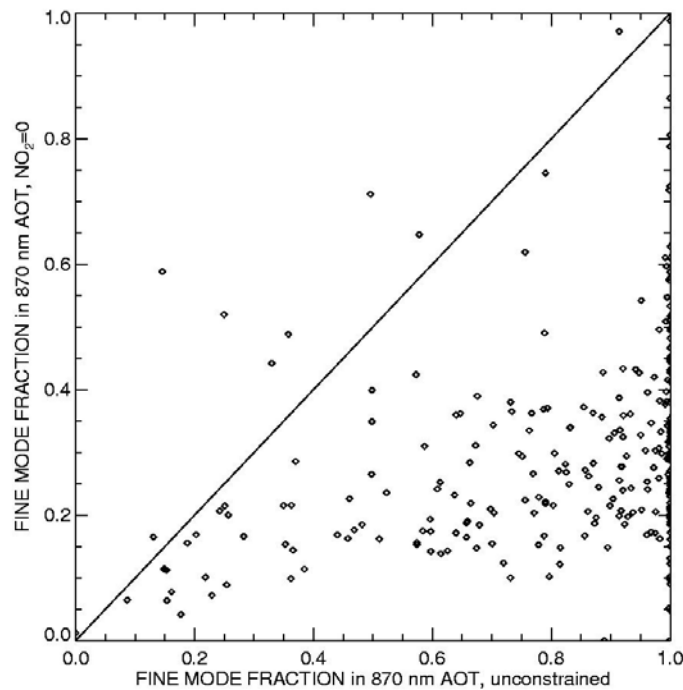


**Figure 1.** Comparison between the fine mode fractions in 870 nm AOT obtained using constrained (zero  $\text{NO}_2$ ) and unconstrained methods for SGP Extended Facilities E2 (left) and E13 (right) for the year 2000.

The trade-offs described above are also clearly seen on simulated data. To show this, we used Mie theory to simulate spectral AOT  $\tau(\lambda)$  in 400-900 nm range with 1 nm resolution. AOT at 870 nm was kept equal to 0.2.  $\text{NO}_2$  spectral absorption coefficients  $b(\lambda)$  were smoothed using 10 nm moving window. From these two spectral dependences we created an  $\text{NO}_2$ -independent combination

$$\tau'(\lambda) = \tau(\lambda) - \tau(400 \text{ nm}) (b(\lambda)/b(400 \text{ nm})).$$

Taking a simulated spectral curve  $\tau(\lambda)+b(\lambda) x_{\text{NO}_2}$  (where  $x_{\text{NO}_2}$  is the assumed column amount of  $\text{NO}_2$ ), we compared it with a family of test spectral AOTs with different fine mode size and fine mode fraction in 870 nm AOT. The measures of agreement are (1) the mean absolute difference between the simulated and the test  $\tau'(\lambda)$  (shown in Figure 2 by solid thick contour line for 0.001 value, solid thin contour line for 0.002, dashed line for 0.005, and by dotted line for 0.01), and (2) the amount of  $\text{NO}_2$  that is needed to be added to the test AOT to match the value of the simulated curve at 400 nm (shown by shades corresponding to amounts from 0 to 8 DU with 2 DU spacing, the left edge of the darkest shade corresponds to zero  $\text{NO}_2$  amount). The parameters of the simulated spectral curve correspond to coordinates of the intersection of the vertical and horizontal dashed lines. The plots show that when a large amount of  $\text{NO}_2$  is used in simulation, the “best estimate” assuming zero  $\text{NO}_2$  amount (shown by intersection of two dotted lines) is in the region with smaller fine mode size and lower fine fraction in AOT. Comparing the right and left plots, we see that uncertainty in fine mode size (and fine mode AOT fraction) increases with the fine particle size. It can be also shown that this uncertainty also increases with a decrease of the fine mode fraction in AOT (since the fine mode properties are then less pronounced), while  $\text{NO}_2$  can be retrieved more accurately since its trade-offs with the fine mode aerosol become smaller.

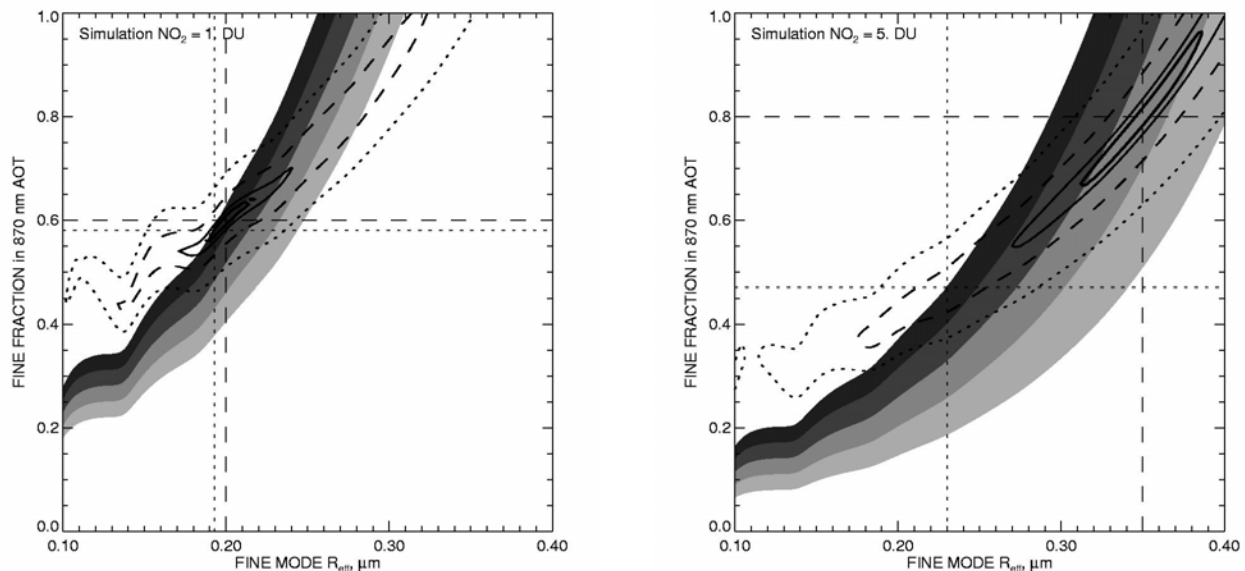


**Figure 2.** Illustration of the trade-offs between  $\text{NO}_2$  and aerosol fine mode radius and fraction in 870 nm AOT using simulated data. The model parameters are (left)  $r_{\text{eff}} = 0.2 \mu\text{m}$ , fraction 0.6,  $\text{NO}_2$  column 1 DU; (right)  $r_{\text{eff}} = 0.35 \mu\text{m}$ , fraction 0.8,  $\text{NO}_2$  column 5 DU. The mean absolute difference between the simulated and the test optical thickness is shown in the plot by solid thick contour line for 0.001 value, solid thin contour line for 0.002, dashed line for 0.005, and by dotted line for 0.01. The amounts of  $\text{NO}_2$  needed to be added to the test AOT to match the value of the simulated curve at 400 nm are shown by shades corresponding to amounts from 0 to 8 DU with 2 DU spacing (the left edge of the darkest shade corresponds to zero  $\text{NO}_2$  amount). The parameters of the simulated spectral curve correspond to coordinates of the intersection of the vertical and horizontal dashed lines, while the “best estimate” assuming zero  $\text{NO}_2$  amount corresponds to intersection of the two dotted lines.

## Retrieval of Aerosol Absorption Properties from MFRSR Data

To retrieve aerosol absorption properties, such as the imaginary part of refractive index and SSA, we use both direct and diffuse spectral irradiances measured by the MFRSR. The retrieval algorithm is based on compatibility between the ratios of direct and diffuse irradiances (direct-diffuse ratios) and corresponding optical thicknesses. A plane-parallel adding-dubbing code has been used to compute a look-up table of diffuse transmission functions depending on solar zenith angle, AOT at 870 nm, fine mode fraction in 870 nm AOT, fine mode effective radius, NO<sub>2</sub> column amount, and the imaginary part of refractive index. A separate table for SSA depending on the above parameters had been also computed. Rayleigh scattering was accounted for in the radiative transfer model, while ozone absorption was not taken into account, since the overwhelming part of ozone is located above aerosol layer, thus its absorption cancels out in direct-diffuse ratio (our tests supported this conclusion). The values of aerosol parameters (and NO<sub>2</sub> in unconstrained algorithm) had been derived using our previously published method (Alexandrov et al. 2005). Surface albedos used in computations were taken from two-year MODIS composite product (A. Trishchenko, private communication).

The preliminary results of aerosol SSA retrievals are presented in Figure 3 as plots of time series of daily mean values for September 2000. Data from the SGP's Central Facility MFRSRs (C1 and E13) have been used. Figure 3 also shows SSA values obtained through AERONET's almucantar scan analysis of data from CIMEL sun-photometer collocated with the two MFRSRs. Although the SSA values from both MFRSRs are consistent with each other, the presented time series exhibits significant difference between MFRSR and AERONET values, with MFRSR's retrievals being systematically lower. As one can see comparing the top and bottom plots of Figure 3, the MFRSR-derived SSAs are especially low when AOT is low (lower than 0.1 at 870 nm), so that the diffuse irradiance is low compared to the direct beam (direct normal exceeds diffuse horizontal by a factor greater than 15). It is clear that the smaller the amount of aerosol studied the greater uncertainty in its retrieved properties. However, this logic does not justify the large systematic bias observed in Figure 3, for which we currently do not have a satisfactory explanation. Our working assumption is that the shadowbanding process (including the two 9 degree off-sun correction measurements) cannot separate direct and diffuse irradiances sufficiently well, and that the error affects the diffuse measurement more than the direct. We plan to perform a sensitivity study with actual modeling of shadowband operation to estimate (and possibly correct for) the "shadowbanding error" under various atmospheric conditions. Another anomaly seen in Figure 3 is the inversion in the spectral dependence of SSA: while its values decrease with wavelength in first four channels, the SSA in the 870-nm channel is greater than this in the 670-nm channel. We continue to work on improvement of our SSA retrievals and on detection of possible instrumental problems, which may affect them.

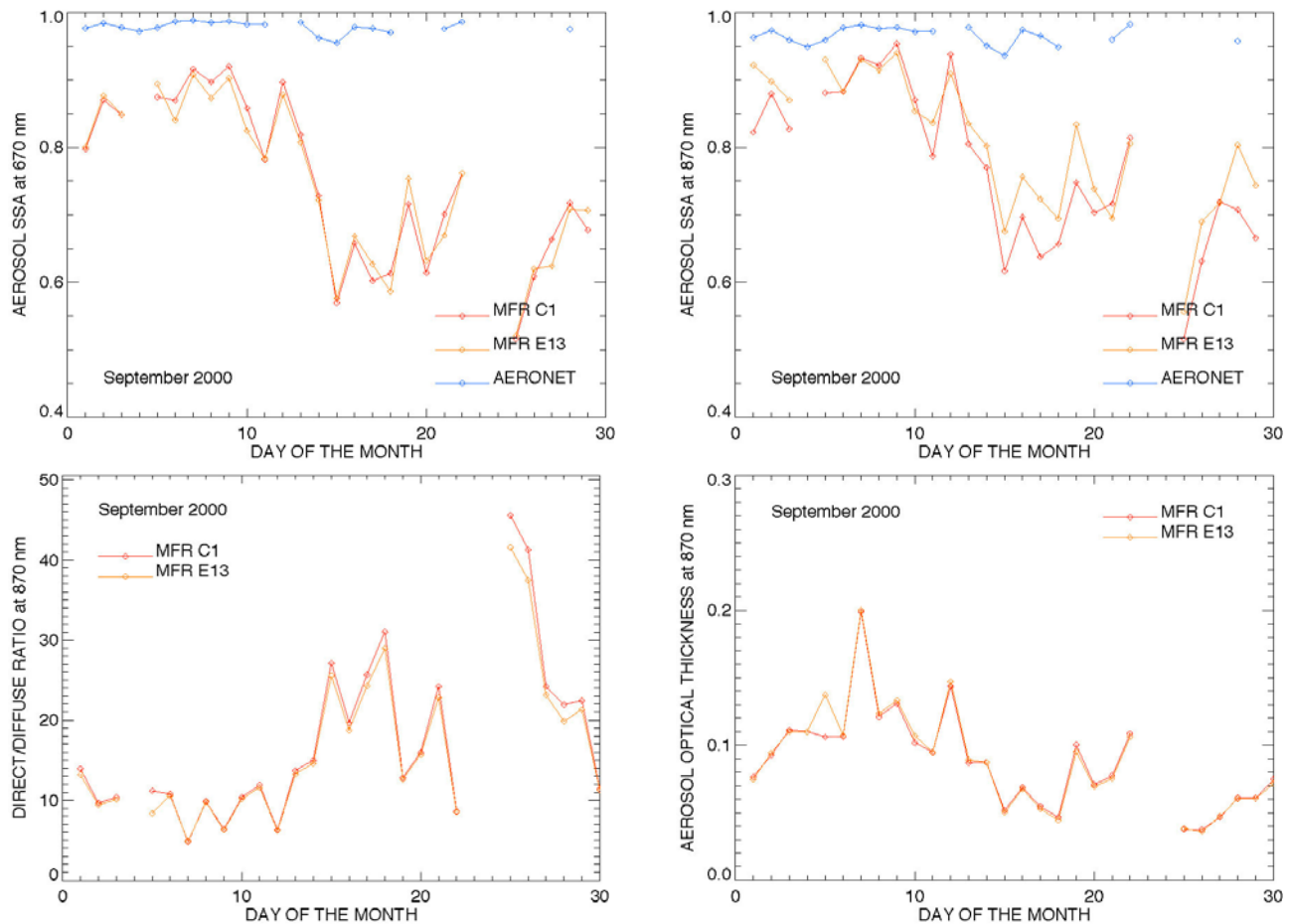


**Figure 3.** Top: time series of daily mean values of aerosol SSA (in 670 and 870 nm channels) retrieved from measurements by SGP Central Facility MFRSRs (C1, E13) made in September 2000 (preliminary results). AERONET's values from almucantar scan analysis are shown for comparison. Constrained (zero  $\text{NO}_2$ ) MFRSR analysis algorithm had been used for these plots. Bottom: corresponding time series of the ratio between direct normal and diffuse horizontal irradiances (left), and aerosol optical thickness in the 870-nm channel.

## Retrievals of Column Amounts of Precipitable Water Vapor

The MFRSR measurements of direct normal irradiances in the 940-nm channel can be used for retrieval of PWV column (Michalsky et al. 1995; Schmid et al. 2001). We performed retrievals of PWV column amounts for the data from all the SGP extended facilities for the year 2000. Figure 5 shows examples of these retrievals for the Central Facility MFRSRs (C1, E13) in comparison with correlative data from the MWR (C1), GPS station from Wind Profiler Demo Network, and AERONET ("Cart-Site" location).

The main problem in the recent years with spectral retrievals of PWV in the visible part of the spectrum has been related to uncertainties in spectral databases. To illustrate these uncertainties we compare in

Figure 4 the growth curves (940 nm slant optical depth of PWV vs slant PWV column) computed for MFRSR head 922 installed on C1 instrument during the year 2000 using four different spectral databases (HITRAN 96, 2000, 2004 and the ESA database). These curves differ quite significantly from each other and from the “experimental” curve (MFRSR-derived slant optical thickness with AOT subtracted versus C1 MWR-derived PWV slant column). However, the two most recent databases, HITRAN 2000 and 2004, yield almost identical results. This encouraged us to assume that the evolution of the spectral databases is in its convergence phase, and HITRAN 2004 is acceptably accurate and suitable for long-term multi-site retrievals.

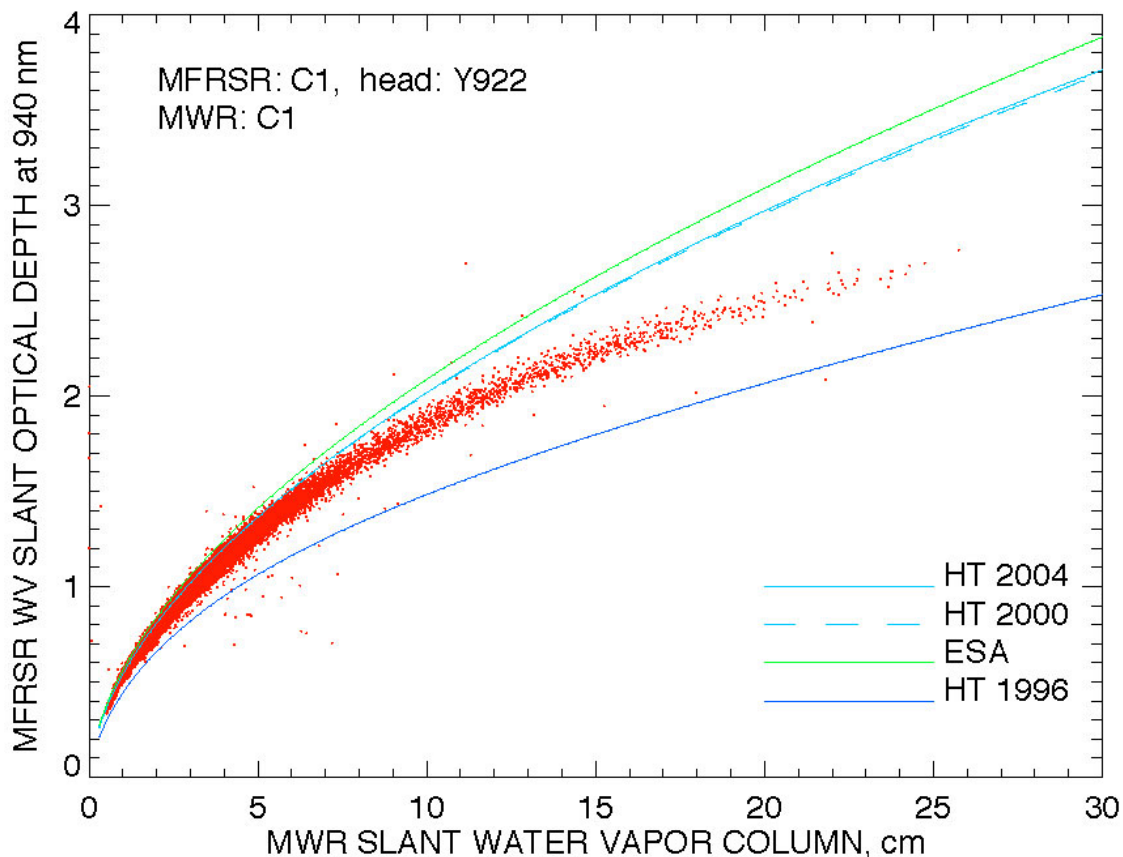


**Figure 4.** Experimental growth curve constructed by plotting MFRSR-derived slant optical thickness in 940 nm channel (with AOT subtracted) vs MWR-derived slant PWV column (SGP Central Facility, 2000). The growth curves obtained by integrating MFRSR spectral response functions with water vapor absorption spectra from various databases (HITRAN 1996, 2000, 2004, European Space Agency (ESA)) are shown by solid lines.

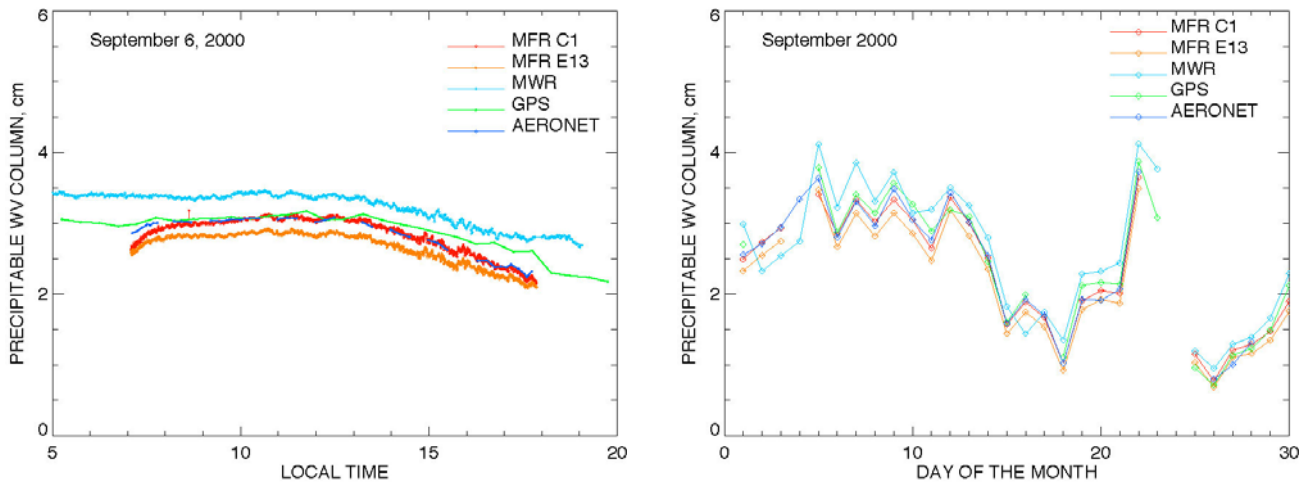


**Figure 5.** Retrievals of column PWV from September 2000 data from the two MFRSRs at SGP’s Central Facility (C1 and E13) in comparison with the correlative data from MWR, GPS, and AERONET. Left: single day (September 6) time series, right: daily mean values for the whole month. C1 data appears to be almost indistinguishable from AERONET retrievals and in better agreement with GPS than with MWR, which yields systematically higher values.

The systematic difference between C1 and E13 values in Figure 5 is likely due to uncertainties in 940 nm channel spectral responses. Comparisons presented in Figure 6 show that C1 MFRSR retrievals appear to be very close to AERONET values (2% bias) and in better agreement with GPS (3% bias) than with MWR (11% bias), which yields systematically higher values. Given high spatial and temporal variability of PWV column, this level of disagreement seems to be acceptable (i.e., measurement uncertainty is not higher than the sampling error due to the choice of measurement time and/or location).

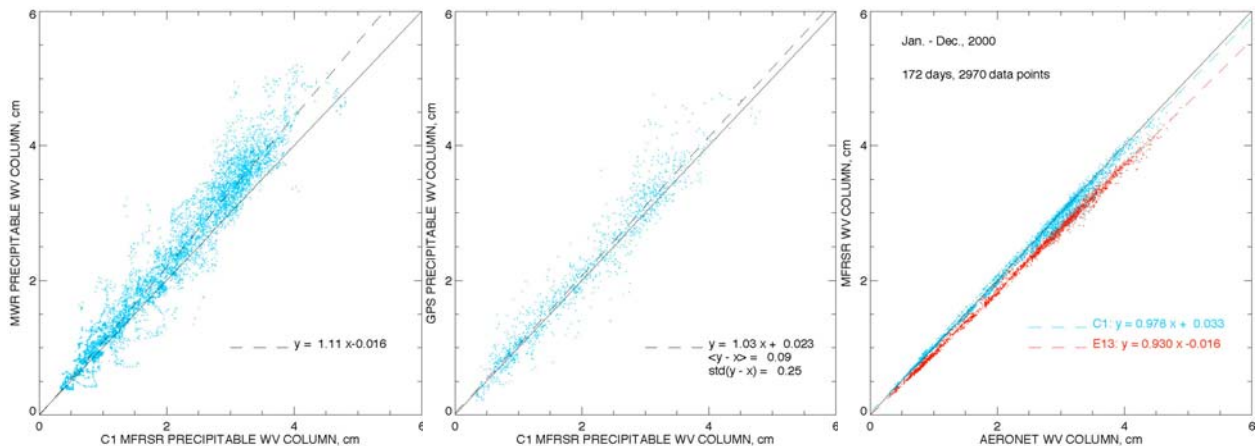


**Figure 6.** Comparison between column PWV retrievals from C1 MFRSR and those from co-located MWR (C1), Wind Profiler Demo Network GPS station, and AERONET’s CIMEL sun-photometer (Cart\_Site). While MWR values show 11% bias compared to C1 MFRSR, GPS and AERONET results are in better agreement with C1 (respectively 3 and 2% bias).

Spatial density of the SGP MFRSR network allows us to reliably interpolate between PWV values obtained at the measurement locations to produce an estimate spatial distribution of water vapor over the area. Figure 7 shows such a spatial distribution constructed from the MFRSR data obtained at noon on September 14, 2000, in comparison with MODIS satellite PWV product for the same time. It is clearly seen that, while lacking small-scale details, the MFRSR network provides accurate spatial structure of PWV. The spatial and temporal structures of MFRSR and MODIS datasets for the SGP area complement each other. While MODIS provides high spatial resolution at a single time moment for a given day, MFRSRs measurements, being more spatially sparse, are made continuously in time. This presents an opportunity for future data fusion between the two datasets.

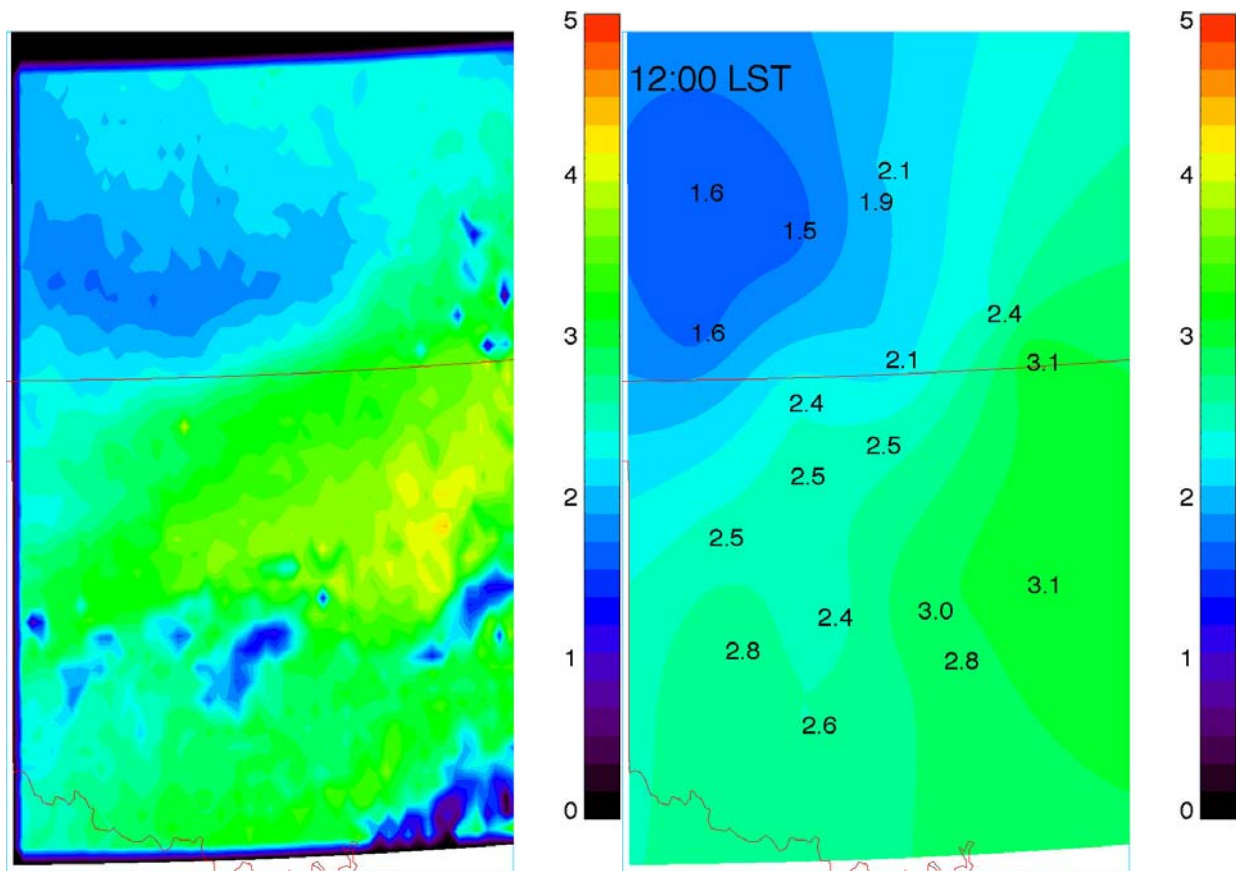


**Figure 7.** MODIS Level 2 water vapor product over SGP site (left) and spatial structure obtained by interpolation of MFRSR network data (left) from 12:00 noon on September 14, 2000. The numbers show the PWV column values (in cm) for each MFRSR location.

## Contact

Mikhail Alexandrov, [malexandrov@giss.nasa.gov](mailto:malexandrov@giss.nasa.gov), phone (212) 678-5548.

## References

Alexandrov, MD, BE Carlson, AA Lacis, and B Cairns. 2005. "Separation of fine and coarse aerosol modes in MFRSR datasets." *Journal of Geophysical Research* 110:D13204.

Michalsky, JJ, JC Liljegren, and LC Harrison. 1995. "A comparison of sun photometer derivations of total column water vapor and ozone to standard measures of same at the Southern Great Plains Atmospheric Radiation Measurement site." *Journal of Geophysical Research* 100:25995 – 26003.

Schmid, B, JJ Michalsky, DW Slater, JC Barnard, RN Halthore, JC Liljegren, BN Holben, TF Eck, JM Livingston, PB Russel, T Ingold, and I Slutsker. 2001. "Comparison of columnar water-vapor measurements from solar transmittance methods." *Applied Optics* 40:1886 – 1896.